Visualization of retrovirus budding with correlated light and electron microscopy

Daniel R. Larson*†‡, Marc C. Johnson†§, Watt W. Webb*¶, and Volker M. Vogt§¶

Departments of *Applied and Engineering Physics and §Molecular Biology and Genetics, Cornell University, Ithaca, NY 14853

Edited by John M. Coffin, Tufts University School of Medicine, Boston, MA, and approved September 15, 2005 (received for review June 8, 2005)

We have used correlated scanning EM (SEM) and multiphoton fluorescence microscopy to visualize budding of virus-like particles (VLPs) of Rous sarcoma virus (RSV) and HIV type 1 (HIV-1). When the Gag structural protein was expressed alone as a GFP fusion, most budding particles appeared morphologically aberrant, but normal assembly could be rescued by coexpression of untagged Gag protein. Imaging of live cells allowed budding to be seen in real time as the disappearance of fluorescent spots from the dorsal cell surface. The disappearance of very bright spots containing clusters of VLPs often occurred in a stepwise fashion. Even after imaging times >1 h, only a minority of the spots disappeared, suggesting that some might be budding-incompetent complexes. On individual cells, we enumerated both the fluorescent puncta and the budding structures visible by SEM and compared these numbers for WT Gag proteins and for Gag proteins that were blocked at the last step in budding by a late domain mutation. For the mutant HIV-1 and RSV proteins, almost all of the fluorescent spots corresponded to budding structures. For WT RSV, the dorsal side of cells showed 3-fold more fluorescent spots than budding structures, suggesting that formation of the polymerized Gag shell precedes bulging out of the membrane. For WT HIV-1, most fluorescent spots corresponded with budding structures, consistent with the slower budding rate of this virus. Combining these two types of microscopy will allow innovative approaches for elucidating the mechanism of retrovirus budding.

assembly | Gag | multiphoton | fluorescence | tracking

Retroviruses encode a single structural polyprotein, Gag, which is the only viral component required for the assembly of a virus-like particle (VLP). The final step in the assembly pathway is the pinching off and release of the VLP from the host cell membrane, an event that is facilitated by the cellular ESCRT (endosomal sorting complex required for transport) complexes (1). Retroviruses recruit ESCRT proteins to budding sites through interaction with a short, 4-aa sequence in Gag known as the late (L) domain (2). Because most retroviruses can be viewed at different stages of assembly on the plasma membrane by thin-section transmission EM, it has generally been assumed that assembly occurs exclusively on the plasma membrane. However, several recent reports have suggested that Gag assembly, at least in some situations, initiates by budding at internal vesicles such as the multivesicular body, the normal site of ESCRT function (3–8).

A challenge in virology is combining the high resolution of EM with the power of fluorescence imaging of live cells. By fluorescence microscopy, the Gag protein shows a punctate pattern that has often been interpreted to represent sites of virus budding, although this interpretation has not been verified directly in quantitative terms. Scanning EM (SEM) is able to resolve individual viral budding structures, but only on the surface of fixed cells. Until now, it has been difficult to merge the high-resolution, static information from SEM with the lower resolution fluorescence information from living cells to generate a comprehensive picture of retrovirus assembly and budding. In this report, we describe correlated SEM and multiphoton laser scanning microscopy (MPM) to observe the late stages of virus budding of Rous sarcoma virus (RSV) and HIV type 1 (HIV-1). The particles were fluorescently labeled by Gag-GFP fusion proteins expressed in the presence of an excess of normal Gag protein. We were able to observe in real time the budding of single VLPs from living cells. By correlated microscopy, a fraction of the fluorescent spots corresponded to spherical budding structures visible on the plasma membrane by SEM. The ability to view the same cell both by MPM and SEM will facilitate studies not only of virus budding but also of other cell surface phenomena.

Materials and Methods

Cell Culture. The chicken fibroblast cell line DF-1 was maintained as described in ref. 9. In some experiments, cells were infected with and stably expressed RSV derived from the RCAS provirus, which is an engineered strain lacking the *v-src* oncogene. Transient transfections were performed by using FuGENE (Roche Diagnostics). For correlative experiments, cells were plated onto gridded coverslips (MatTek, Ashland, MA) before transfection and viewed 24–48 h posttransfection.

Vectors. The RSV Gag-GFP construct is described in refs. 9 and 10 and is based on the enhanced fluorescent version of this protein (EGFP). Equivalent constructs missing their L domain (denoted by GagΔL) were created by changing the PPPY sequence to AAAA. The HIV-1 Gag-GFP construct is described in ref. 11 and was kindly provided by Marilyn Resh (Memorial Sloan–Kettering Cancer Center, New York). HIV-1 Gag, HIV-1 GagΔL, and HIV-1 GagΔL-GFP were created by introducing a stop codon after the last codon of p6 and/or changing the PTAP sequence to AAAA.

EM. Cells to be viewed by both MPM and SEM were fixed in PBS plus 4% paraformaldehyde before MPM. After fluorescence imaging, cells were fixed in 0.2 M phosphate buffer (pH 7.2) plus 2.5% glutaraldehyde, postfixed in 2% osmium tetroxide, dehydrated in ethanol, critical point-dried, and sputter-coated with gold palladium for 60 s. Cells were identified by their location on a finder grid and imaged by using a LEO 1550 field-emission scanning electron microscope (LEO, Helsingborg, Sweden) at 3 kV.

Image Acquisition and Analysis. All fluorescence live cell images were acquired on a home-built two-photon laser scanning microscope that is described in refs. 9 and 12. All tracking analysis was done by using custom software developed with IDL 6.0

Conflict of interest statement: No conflicts declared.

This paper was submitted directly (Track II) to the PNAS office.

Abbreviations: VLP, virus-like particle; L, late; SEM, scanning EM; MPM, multiphoton laser scanning microscopy; HIV-1, HIV type 1; RSV, Rous sarcoma virus.

†D.R.L. and M.C.J. contributed equally to this work.

‡Present address: Department of Anatomy and Structural Biology, Albert Einstein College of Medicine, Bronx, NY 10461.

¶To whom correspondence may be addressed. E-mail: www2@cornell.edu or vmv1@cornell.edu.

© 2005 by The National Academy of Sciences of the USA

Downloaded by guest on October 22, 2020

BIOPHYSICS

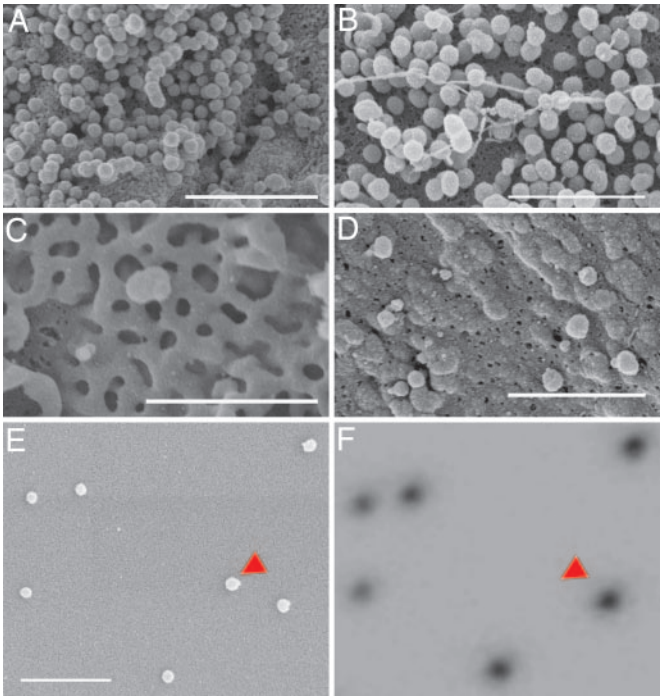

Fig. 1. Budding of Gag-GFP is abnormal unless Gag is coexpressed. (*A–D*) SEM images show representative cells expressing RSV Gag plus RSV Gag-GFP (*A*), HIV-1 Gag plus HIV-1 Gag-GFP (*B*), RSV Gag-GFP alone (*C*), and HIV-1 Gag-GFP alone (*D*). (*E*) SEM micrograph of VLPs on a gridded coverslip (the grid is not visible). (*F*) Confocal image of the same region. The red arrowhead indicates a particle that is visible in the SEM image but not in the fluorescence image. (Scale bars, 1 μm.)

(Research Systems, Boulder, CO). The tracking algorithm is based on: (*i*) a localization routine to find the center and intensity of each spot as described in ref. 13 and (*ii*) a tracking routine based on ref. 14.

For correlated SEM and MPM, fixed cells were first imaged by acquiring sequential *z* planes. Because the bottom of the cell is not visible by SEM, the ventral planes (the surface of the cell in contact with the coverslip) were removed, and the remaining planes were maximum-projected into a single 2D image. The MPM images were enlarged until the scale bar matched the scale bar on the SEMs. No further resizing was done. The SEM image was made to "resemble" the fluorescence image by superimposing a spot with the dimensions of the optical point spread function on the position of each virus identified by SEM. Then, the fluorescence image was translated and rotated with PHOTOSHOP (Adobe Systems, San Jose, CA) to bring it into registry with the SEM. Fluorescent virus counting was done by using the tracking software. SEM virus counting was performed by hand.

Results

Properly Formed VLPs Containing Untagged Gag and Gag-GFP Can Be Enumerated on the Cell Surface and the Substratum. Late stages of retrovirus assembly for RSV and HIV-1 are visible by SEM as curved budding structures that resemble marbles present on the cell surface (Fig. 1 *A* and *B*). When Gag was expressed by itself or coexpressed with Gag-GFP, these VLPs were uniform in size and shape. Their distribution appeared nonrandom, often with high concentrations on one edge of the cell or over the main cell body, but with very few VLPs in flat parts of the cell away from the main cell body. Expressing Gag-GFP by itself, without unlabeled Gag, resulted in a variety of aberrant structures for both RSV and HIV-1 (Fig. 1 *C* and *D*). Although some normal particles also were present on these Gag-GFP-expressing cells, the majority of the cell displayed honeycomb-like structures for RSV (Fig. 1*C*) or structures resembling submembrane bulges for HIV-1 (Fig. 1*D*). These aberrant formations were eliminated by cotransfection of at least a 3-fold excess of DNA coding for RSV Gag without the GFP tag and at least a 10-fold excess for HIV-1 Gag. Therefore, all experiments presented here were carried out with a mixture of Gag-GFP and untagged Gag, the latter being derived either by cotransfection or by expression in cells stably infected with RSV.

Fluorescent puncta were observed not only associated with cells but also on the glass surface. Those observed on the glass surface were relatively uniform in intensity, suggesting incorporation of Gag and Gag-GFP at approximately the same levels. The spots on the glass could be definitively identified as VLPs by SEM (Fig. 1 *E* and *F*). In this experiment, all of the cells were infected with RSV, but only some of them became transfected, thus explaining the presence of some nonfluorescent particles (Fig. 1*F*, red arrowhead). Many VLPs appeared to have budded from the ventral surface of an adherent cell (the surface in contact with the coverslip) and remained stuck to the glass, as shown by EDTA treatment, which caused the cells to round up and eventually detach but left many of the spots on the coverslip [see Fig. 5 (red arrowheads) and Movie 1, which are published as supporting information on the PNAS web site]. The same phenomenon also was observed in a migrating cell (Movie 2, which is published as supporting information on the PNAS web site). We interpret these results to mean that an appreciable fraction of viruses bud from the ventral surface and that some of the particles visible on the coverslip exited the cell in this manner.

Taken together, these results demonstrate that proper assembly of Gag-GFP requires excess unlabeled Gag, that Gag and Gag-GFP coassemble into particles that bud from the host cell and are visible by SEM and MPM, and that budding can occur from the ventral surface of the cell. Thus, Gag-GFP plus a "driver" Gag can be used as a model system to observe budding events in living cells.

Real-Time Visualization of RSV Budding. To observe budding events from living cells, we found it necessary to image the cell for long periods of time (>2 h) at moderate frame rates (one frame every 10 s) with the option of acquiring *z* stacks at each time point (eight image planes per cell), without significant photobleaching. To meet these stringent experimental constraints, we used a custom two-photon microscope optimized for sensitivity and low drift. Budding events observed in this manner are shown in Fig. 2.

MPM of RSV-infected DF-1 cells expressing RSV Gag-GFP from a transfected plasmid showed the familiar punctuate pattern both outside and inside the borders of the cell, with an additional diffuse Gag-GFP fluorescence within the cell (Fig. 2*A*), as reported previously by many investigators. The Fig. 2*A* *Inset* is the magnified region demarcated by the green dashed box at a time 405 s later; the trajectory of a particle that would eventually bud is superimposed in red. The trajectory is the path of the particle from the 405-s time point to the budding event ≈1,300 s later. The only signature of a budding event is the disappearance of a spot within a single frame. The integrated fluorescence intensity of this budding particle (Fig. 2*B*) remained constant over its entire trajectory, with no increase in fluorescence as might be expected if one were observing Gag plus Gag-GFP assembly into the particle before its release (see also Movies 3 and 4, which are published as supporting information on the PNAS web site).

The disappearance of a fluorescence spot is only circumstantial evidence that a budding event occurred. To control for possible gross fluctuations in the membrane and for other aberrations, we looked at clusters of closely spaced fluorescent

Downloaded by guest on October 22, 2020

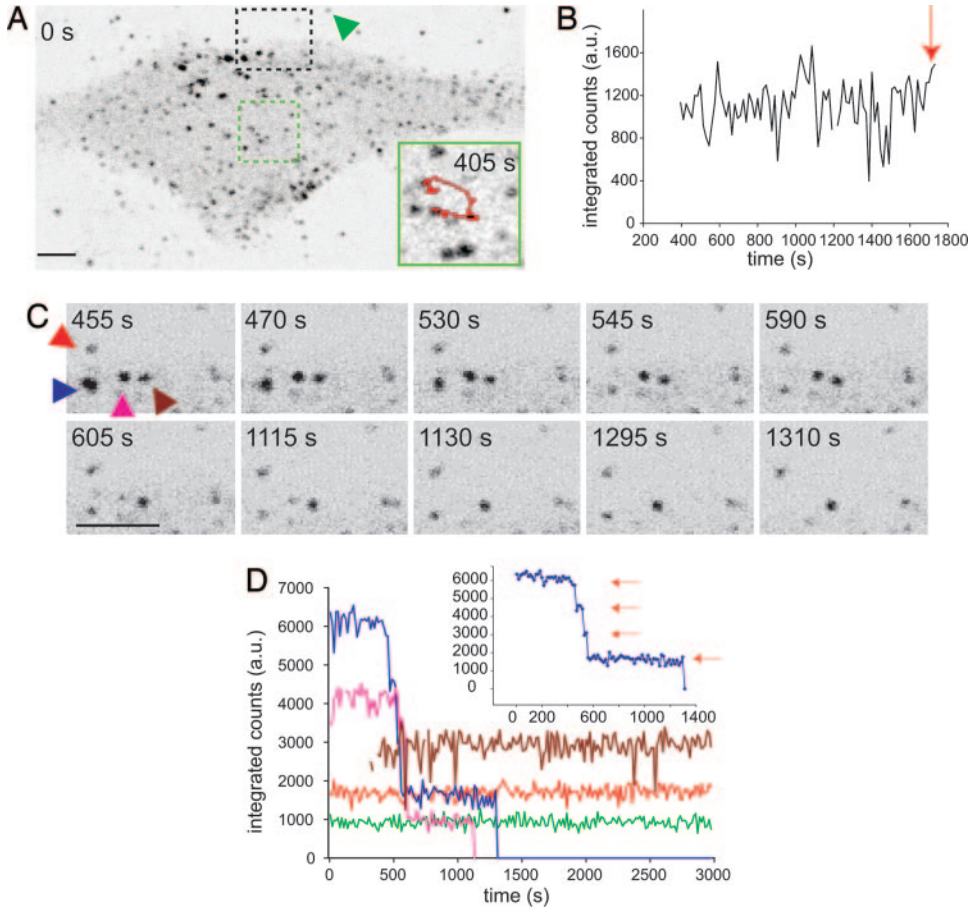

Fig. 2. RSV budding can be visualized in real time. (*A*) Multiphoton image of a DF-1 cell. *Inset* is a blowup of the region demarcated by the green dashed box at a time point of 405 s. The red trace is the spatial trajectory of a particle that would bud from the cell at ≈1,700 s. (*B*) Integrated intensity (brightness) of the particle trajectory shown in *A Inset*. The red arrow indicates the point where the particle disappears. (*C*) Selected time points for the region demarcated by the black dashed box in *A*. The colored arrowheads indicate particles (or clusters of particles) that disappear in the subsequent frames. (*D*) Intensity traces for the particles in *C*. Line color corresponds to arrowhead color. *Inset* is the single trace for the blue particle. (Scale bars, 5 μm.)

spots (Fig. 2*C*, which shows a magnified region of the black dashed box in Fig. 2*A*). A few time frames have been selected to show the sequential disappearance of virus particles from this region. Four spots are indicated by colored arrowheads, and the intensity traces are shown in the same color in Fig. 2*D*. The green spot is a single particle stuck to the coverslip and is a control for drift and photobleaching. Both the blue particle and the pink particle have an initial brightness that is much greater than a single particle, indicating possible clusters. The intensities of these traces (blue and pink) show stepwise decreases in fluorescence, with the size of the steps corresponding to the intensity of a single particle, ≈1,000 counts. These stepwise decreases can also be seen in the images (for example, the pink particle at 455, 605, and 1,130 s) (Fig. 2*C*). The sequential disappearance is more clearly evident in Fig. 2*D Inset*, which is the intensity time trace of the blue particle. The facts that the fluorescence disappears in discrete steps and that spots in the same localized area (Fig. 2*C*, brown and red) remain constant argue against the possibility that objects have left the field of view or become bleached. Thus, we interpret each of the stepwise diminutions in intensity to represent the release of a single VLP.

A striking feature of this real-time imaging was the relatively small fraction of fluorescent spots that disappeared, indicating budding. Many of the spots on the cell persisted for hours, exhibiting a wide range of motion and behavior but never disappearing in discernible budding events. The same was true for HIV-1 (data not shown). To investigate what these fluorescent moieties might be, we turned to a combination of SEM and MPM.

Correlated SEM and MPM of RSV. With a combined SEM and MPM approach, it is possible to correlate the distribution of Gag-GFP puncta (both inside the cell and on the surface) with the late budding viral structures observed by SEM. In brief, cells cotransfected with DNAs encoding Gag and Gag-GFP first are lightly fixed and imaged by MPM. The MPM images are *z* stacks with the ventral surface removed and projected into a single 2D image (see *Materials and Methods*). The cells are then prepared for SEM, located by means of an etched coverslip grid, and then imaged. One goal of these experiments was to ascertain what fraction of the fluorescent puncta actually represent budding virus particles at the cell surface. We carried out such experiments both with cells expressing WT RSV Gag/Gag-GFP and with cells expressing the same pair of proteins that both carry an L domain mutation, with the PPPY motif in RSV Gag changed to AAAA (GagΔL/GagΔL-GFP). It is known that cells expressing L domain mutations accumulate budding virus particles that remain tethered to the membrane (2).

An example of this analysis for RSV GagΔL/GagΔL-GFP is presented in Fig. 3. The composite SEM shows most of the surface of a single cell (Fig. 3*A*; an enlarged view of the yellow boxed area with a high density of particles is shown in Fig. 3*F*).

Downloaded by guest on October 22, 2020

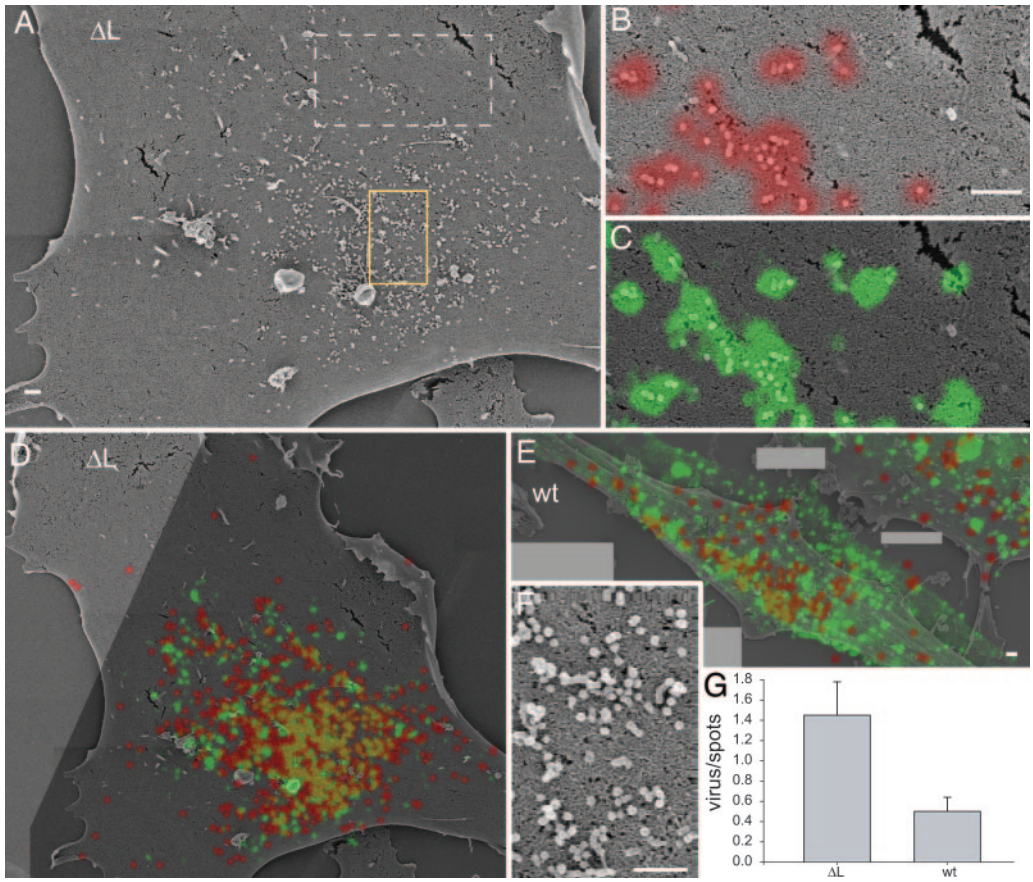

Fig. 3. Correlation of SEM and MPM reveals the fraction of the RSV fluorescent puncta that are budding particles on the cell surface. (*A*) Composite SEM image of a cell coexpressing GagΔL/GagΔL-GFP. (*B*) Region of *A* demarcated by the white dashed box. Red overlay is a pseudofluorescence image generated by making each viral particle appear as a diffraction-limited fluorescent spot. (*C*) Same region as in *B*, but the green overlay is the actual volume-projected GFP image. (*D*) Full-field merge of red pseudofluorescence and green GFP for the cell in *A* ($P = 0.61$). (*E*) Full-field merge of a cell coexpressing Gag/Gag-GFP ($P = 0.36$). (*F*) Region of *A* demarcated by a yellow box showing particles at higher magnification. (*G*) Compilation of the ratio of virus particles/fluorescent spots (i.e., red spots/green spots): GagΔL/GagΔL-GFP, $n = 6$; Gag/Gag-GFP, $n = 8$. Error bars are the standard error of the mean. (Scale bars, 1 μm.)

A region of the SEM image selected for its moderate density of particles (Fig. 3*A*, white dashed box) is shown with a red pseudofluorescence overlay (Fig. 3*B*). The corresponding green fluorescence GFP image is remarkably similar, given the perturbative effects of SEM processing (Fig. 3*C*, which is magnified as in Fig. 3*B*, and Fig. 3*D* at full field). Almost all of the visible VLPs are green by fluorescence, although there are some green spots not visible by SEM. Even at full field, a high degree of correspondence between the green fluorescent image and the red pseudofluorescence image is apparent (as quantified by the Pearson correlation coefficient $P = 0.61$). Most deviations are consistent with the shrinkage and contraction of the cell due to fixation and drying. In summary, for cells expressing RSV GagΔL/GagΔL-GFP, almost all of the fluorescent spots corresponded to identifiable budding structures on the dorsal surface of the cell.

For cells expressing WT Gag/Gag-GFP proteins, the correspondence between the green GFP image and the red pseudofluorescence image was diminished. In the example shown (Fig. 3*E*), DF-1 cells infected with RSV were transfected with a DNA expressing Gag-GFP. Many more green spots are visible than budding virus particles, with large fluorescent patches present in areas almost devoid of VLPs ($P = 0.36$). We interpret these data to mean that Gag/Gag-GFP assembly can occur inside the cell, presumably on vesicles or possibly underneath the plasma membrane without the membrane bulging out.

A more robust measure of correlation can be obtained by simply counting the number of budding virus particles on the surface and comparing this number with the number of green spots. This method does not depend on the fidelity of the overlay between the SEM and MPM images and requires only that the same cell be found in both MPM and SEM. The virus/spots ratio was 1.2 for the GagΔL/GagΔL-GFP cell (Fig. 3*A*) and 0.37 for the Gag/Gag-GFP cell (Fig. 3*E*), in agreement with the correlation coefficients. The average ratio compiled from multiple cells was almost unity for ΔL cells and 0.5 for WT cells (Fig. 3*G*). The fact that the ratio is >1, meaning that there seem to be more viruses than green spots, probably is due to the difficulty in accurately counting the green spots when they are at high density.

In total, for eight cells, 43% of the spots in the cell were located in the ventral confocal sections, where budding events would not be visible by SEM (data not shown). Of the remaining 57%, approximately one-third corresponded to spherical budding structures by SEM (see above). Therefore, approximately one-fifth of all of the Gag-GFP spots in the fluorescence image might have been poised to disappear by budding from the dorsal membrane. The fraction we actually observed disappear was ≈10-fold lower.

Correlated SEM and MPM of HIV-1. We carried out similar correlative microscopic analyses for cells expressing HIV-1 Gag and Gag-GFP, in context of both WT protein and protein in which the L domain sequence PTAP was ablated. The same avian cell

Downloaded by guest on October 22, 2020

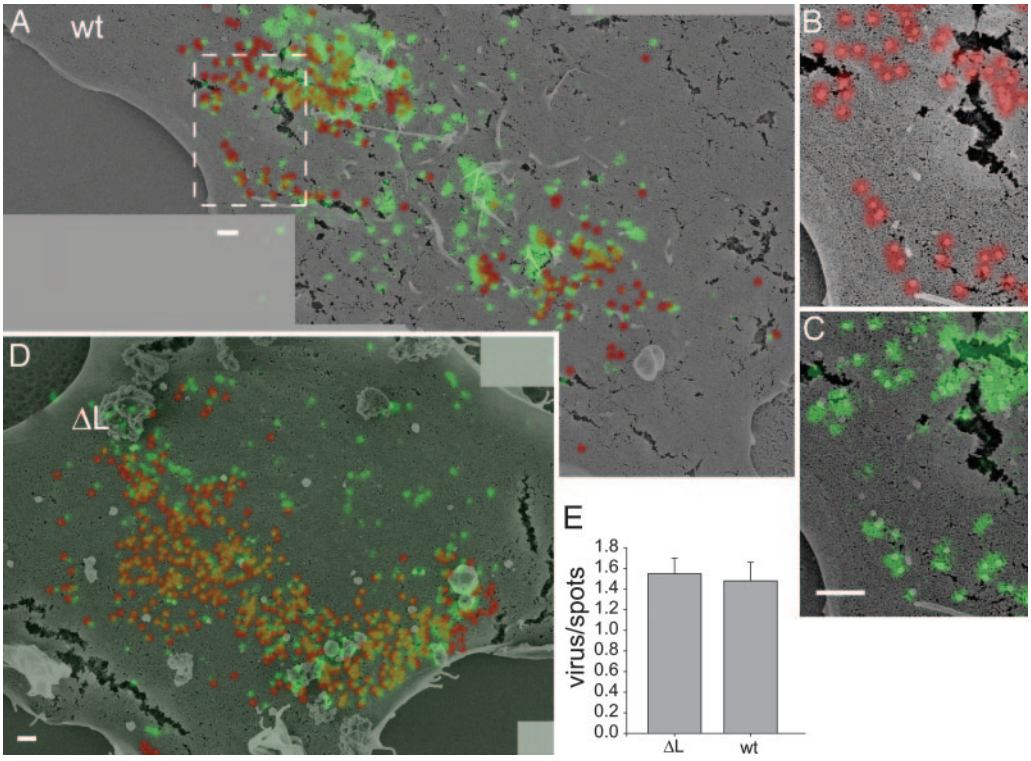

Fig. 4. Correlation of SEM and MPM reveals the fraction of the HIV-1 fluorescent puncta that are budding particles on the cell surface. (*A*) Composite image of a DF-1 cell coexpressing Gag/Gag-GFP. (*B*) Region of *A* demarcated by the white dashed box. The overlay is the red pseudofluorescence image. (*C*) Same region as in *B*, but the green overlay is the actual volume-projected GFP image. (*D*) Composite image of a cell expressing GagΔL/GagΔL-GFP. (*F*) Compilation of the ratio of virus particles/fluorescent spots (i.e., red spots/green spots): GagΔL/GagΔL-GFP, $n = 8$; Gag/Gag-GFP, $n = 8$. Error bars are the standard error of the mean. (Scale bars, 1 μm.)

line (DF-1) was used for consistency and because these cells have an exceptionally smooth plasma membrane that allows reliable visualization of budding VLPs. The cells were cotransfected with DNAs encoding Gag and Gag-GFP, with the former in 20-fold excess. There was a greater degree of correspondence between MPM and SEM for HIV-1 Gag/Gag-GFP ($P = 0.42$) than for RSV Gag/Gag-GFP (Fig. 4*A*). Indeed, there were some regions of very high correlation, as indicated in the *Inset* (pseudofluorescence, Fig. 4*B*; fluorescence, Fig. 4*C*). Likewise, in the case of HIV-1 GagΔL/GagΔL-GFP, there was nearly perfect agreement between the SEM and MPM images, with small differences primarily due to SEM preparation artifacts (Fig. 4*D*) ($P = 0.55$). A comparison of the number of viruses visible by SEM and green spots visible by MPM yielded statistically identical results for WT Gag and GagΔL: Both ratios were close to unity (Fig. 4*E*). In other words, for WT HIV-1 Gag/Gag-GFP, almost all of the foci of assembly demarcated by fluorescent spots are sites of bulging out at the plasma membrane. As discussed below, this difference between RSV and HIV-1 budding most likely is due to the differences in budding rates for the two viruses.

In summary, combining two-photon fluorescence imaging with SEM has allowed us to describe some of the parameters governing Gag assembly and budding for two model retroviruses. When used together, these complementary techniques are able to provide insight not only into virus budding but more generally into cell surface phenomena that are associated with shape changes in the plasma membrane.

Discussion

A primary objective of this study was to characterize the budding of retroviruses in real time *in vivo*. Although entry of single HIV-1 particles has been imaged in live cells (19), we are not aware of similar studies on budding of single particles. We have shown that VLPs bud one at a time from the plasma membrane, occasionally from the same site. Correlated fluorescence microscopy and SEM imaging demonstrated that Gag-GFP can be incorporated into morphologically correct structures in the presence of excess untagged Gag and that a large fraction of the fluorescent spots observed by MPM correspond with properly assembled VLPs.

It has often been assumed that Gag-GFP properly carries out all of the functions of untagged Gag (4, 9–11, 15). Early evidence suggested that, by itself, RSV Gag-GFP formed particles with normal morphology (10). However, from more recent data (Rebecca Craven, personal communication), such particles seem to have heterogeneous sedimentation coefficients, consistent with the aberrant forms we have visualized by SEM. For HIV-1, previously reported thin-section EM of Gag-GFP-expressing cells yielded images of structures resembling immature HIV-1 virions but containing atypical discontinuities in the Gag layer (15). We did observe some properly assembled particles from both RSV and HIV-1 Gag-GFP, and it was only a systematic comparison of the fluorescent and SEM data that led to the conclusion that the majority of cells expressing Gag-GFP produce predominantly aberrant particles. However, coexpression of labeled and unlabeled Gag apparently results in properly assembled particles, providing a model system for studying budding events on living cells.

We observed that the majority of the fluorescent Gag-GFP puncta remained unchanged, even when individual cells were viewed for several hours and budding events were recorded infrequently. Furthermore, we were never able to visualize the formation (i.e., increase in fluorescence) of a fluorescent spot, the expected signature of the polymerization of Gag molecules

Downloaded by guest on October 22, 2020

in the process of forming a prebudding structure. The intensity trajectories (e.g., Fig. 2*B*) remained relatively constant, up to the disappearance indicative of a budding event. What might be the biological relevance of fluorescence spots that do not disappear? Observations of VLP-producing cells by fluorescence and by pulse–chase radioactive labeling lead to conclusions that appear quantitatively inconsistent. Both in transfected cells and in infected cells producing live RSV or HIV-1 virus, half of the Gag protein pulse-labeled for short times with a radioactive amino acid is released in particulate form into the medium within one to a few hours (refs. 11 and 16 and unpublished data). Given this budding rate measured biochemically, one would expect to see frequent budding events by microscopy and a high turnover of Gag-GFP in the cell. Several factors might contribute to the observed discrepancy. First, some of the fluorescent spots may be VLPs that had finished budding but remained stuck to the coverslip or associated with the cell. Second, some spots may represent dead-end complexes (i.e., complexes that are incompetent to bud or that have highly retarded kinetics of budding, perhaps because assembly has occurred on intracellular vesicles). Published data on pulse–chase radioactive labeling of viral proteins do not exclude that a small percentage of Gag-GFP molecules form such complexes. For example, if 10% of newly synthesized Gag-GFP molecules remained in the cell and were not degraded, at steady state, these molecules might represent a majority of all of the Gag-GFP visualized as spots by MPM, because most of the Gag-GFP leaves the cell by budding. Third, the time required for the GFP moiety of Gag-GFP to become fluorescent (maturation) may be of the same magnitude as the half-time of budding. Estimates of the maturation time for GFP itself vary widely (17, 18), and maturation might be slowed by the upstream Gag sequence. We hypothesize that in a cohort of newly translated Gag-GFP molecules, some or many exit the cell as VLPs before becoming fluorescent.

A challenge for electron microscopists has been finding ways to quantitatively correlate EM images with data obtained in other ways. Correlative SEM and MPM is a powerful tool for visualizing cell surface structures at two different resolutions. For the GagΔL/GagΔL-GFP proteins of RSV and of HIV-1, which carry L domain mutations, almost all of the fluorescent puncta corresponded to the marble-like VLPs seen by SEM on the cell surface. For WT RSV Gag, 2- to 3-fold more fluorescent puncta were counted than surface VLPs. In many cases, where areas of the plasma membrane appeared smooth by SEM, it was possible to unambiguously identify particular fluorescent puncta that were inside the cell, presumably corresponding to sites of assembly. Such sites might be internal to the cell (for example, on vesicles) or possibly directly underneath the plasma membrane before it has started to bulge out.

In contrast to WT RSV, the majority of the WT HIV-1 Gag/Gag-GFP fluorescent dots corresponded to assembled VLPs on the plasma membrane. We hypothesize that this difference is due to the slower budding rate of HIV-1. In pulse–chase labeling of Gag-expressing cells, the time for half of the final radioactive viral protein to be released into the medium is ≈1 h for RSV (16) and ≈3 h for HIV-1 (11), numbers that we have confirmed for the DF-1 cells used in this study.

The following model could explain our quantitative analysis of HIV-1 and RSV budding structures and fluorescent puncta. Gag initiates assembly on membranes in a process that is rapid (19), possibly occurring within the maturation time of the GFP chromophore. For RSV, approximately half of the assembled Gag is in a form other than visible budding structures, presumably on internal membranes. For HIV-1, most of the assembled Gag corresponds to surface budding structures, reflecting rapid binding or transport to the plasma membrane in these cells. Budding itself occurs by a two-step process in which the Gag protein shell first bulges out of the membrane to yield a nearly complete particle identifiable by SEM and then is pinched off with the aid of cellular ESCRT (endosomal sorting complex required for transport) machinery. Compared with RSV, HIV-1 completes the first step rapidly, but the second step occurs more slowly, so that a higher proportion of WT HIV-1 Gag is visible as surface particles by SEM. More detailed analyses of the type presented here will be required to test the predictions of this model, with focus on diverse cell types and with tools that allow protein expression levels to be controlled.

This work was supported by National Science Foundation Grant DBI-0080792, National Institute of Biomedical Imaging and Bioengineering–National Institutes of Health Grant 9 P41 EB001976 (to D.R.L. and W.W.W.), and National Institutes of Health Grant CA-20081 (to M.C.J. and V.M.V.). D.R.L. was supported by the Nanobiotechnology Center at Cornell University (ECS-9876771).

1. Pornillos, O., Garrus, J. E. & Sundquist, W. I. (2002) *Trends Cell Biol.* **12,** 569–579.
2. Freed, E. O. (2002) *J. Virol.* **76,** 4679–4687.
3. Pelchen-Matthews, A., Kramer, B. & Marsh, M. (2003) *J. Cell Biol.* **162,** 443–455.
4. Sherer, N. M., Lehmann, M. J., Jimenez-Soto, L. F., Ingmundson, A., Horner, S. M., Cicchetti, G., Allen, P. G., Pypaert, M., Cunningham, J. M. & Mothes, W. (2003) *Traffic* **4,** 785–801.
5. Nguyen, D. G., Booth, A., Gould, S. J. & Hildreth, J. E. K. (2003) *J. Biol. Chem.* **278,** 52347–52354.
6. Basyuk, E., Galli, T., Mougel, M., Blanchard, J.-M., Sitbon, M. & Bertrand, E. (2003) *Dev. Cell* **5,** 161–174.
7. Ono, A. & Freed, E. O. (2004) *J. Virol.* **78,** 1552–1563.
8. Sandrin, V., Muriaux, D., Darlix, J.-L. & Cosset, F.-L. (2004) *J. Virol.* **78,** 7153–7164.
9. Larson, D. R., Ma, Y. M., Vogt, V. M. & Webb, W. W. (2003) *J. Cell Biol.* **162,** 1233–1244.
10. Callahan, E. M. & Wills, J. W. (2000) *J. Virol.* **74,** 11222–11229.
11. Hermida-Matsumoto, L. & Resh, M. D. (2000) *J. Virol.* **74,** 8670–8679.
12. Larson, D. R. (2003) in *Field of Biophysics* (Cornell Univ., Ithaca, NY).
13. Thompson, R. E., Larson, D. R. & Webb, W. W. (2002) *Biophys. J.* **82,** 2775–2783.
14. Crocker, J. C. & Grier, D. G. (1996) *J. Colloid Interface Sci.* **179,** 298–310.
15. Pornillos, O., Higginson, D. S., Stray, K. M., Fisher, R. D., Garrus, J. E., Payne, M., He, G.-P., Wang, H. E., Morham, S. G. & Sundquist, W. I. (2003) *J. Cell Biol.* **162,** 425–434.
16. Wills, J. W., Cameron, C. E., Wilson, C. B., Xiang, Y., Bennett, R. P. & Leis, J. (1994) *J. Virol.* **68,** 6605–6618.
17. Reid, B. G. & Flynn, G. C. (1997) *Biochemistry* **36,** 6786–6791.
18. Waldo, G. S., Standish, B. M., Berendzen, J. & Terwilliger, T. C. (1999) *Nat. Biotechnol.* **17,** 691–695.
19. Tritel, M. & Resh, M. D. (2000) *J. Virol.* **74,** 5845–5855.

Downloaded by guest on October 22, 2020